Noninvasive Quantification of Hepatic Arterial Blood Flow with Nitrogen-13-Ammonia and Dynamic Positron Emission Tomography

Benjamin C. Chen, Sung-Cheng Huang, Guido Germano, William Kuhle, Randall A. Hawkins, Denis Buxton, Richard C. Brunken, Heinz R. Schelbert, and Michael E. Phelps

Division of Nuclear Medicine and Biophysics, Department of Radiological Sciences, UCLA School of Medicine, and Laboratory of Biomedical and Environmental Sciences, University of California, Los Angeles, California

To determine if dynamic PET and ^{13}N-ammonia can be utilized to quantitate regional hepatic arterial blood flow (rHABF) noninvasively, eight anesthetized dogs and eight human volunteers were examined with PET following intravenous bolus administration of ^{13}N-ammonia. Hepatic time-activity curves and the arterial input function were derived from ROIs drawn over the right lateral superior segment of the liver and the left ventricle of the heart, respectively. rHABF was quantitated using a two-compartment model, with comparison with simultaneously acquired microsphere blood flow measurement (MS) in the canine studies. rHABF derived from canine dynamic PET with ^{13}N-ammonia were linearly related to microsphere values (rHABF = 0.92 × MS + 0.04, r = 0.98), with a mean of 0.40 ml/min/g. The results in eight normal volunteers gave a rHABF value of 0.26 ± 0.07 ml/min/g. Dynamic ^{13}N-ammonia hepatic PET allows noninvasive quantification of rHABF.

J Nucl Med 1991; 32:2219–2208

Since various liver diseases alter hepatic arterial circulation (*1*), accurate noninvasive, quantitative determination of hepatic arterial blood flow in humans may enhance our understanding of these disease processes. Several experimental techniques available in the animal model allow quantitative assessment of regional hepatic arterial blood flow (rHABF) under a variety of conditions (*2*). However, most of these techniques are either invasive (e.g., flow probes) or require postmortem analysis of tissue radioactivity (radiolabeled microspheres). Several noninvasive radionuclide scintigraphic techniques have been developed to assess hepatic blood flow (*3*). However, these techniques permit only estimation of the relative contributions of hepatic arterial and portal venous blood flows, or "effective hepatic blood flow" (*3*). With advances in PET, several techniques employing ^{13}N-ammonia, ^{15}O-water or ^{82}Rb have been described for the absolute quantification of myocardial blood flow (*4–8*). In particular, dynamic PET with ^{13}N-ammonia and tracer kinetic modeling permit separation of the initial tracer extraction of ammonia and its subsequent metabolic conversion to glutamine in the myocardium. The liver receives about 25% of the cardiac output, is involved with most of the biochemical metabolism in the body, and is large and relatively homogeneous without much motion. All these factors make it ideal for PET imaging (*9*). Moreover, the high first-pass extraction of ^{13}N-ammonia by the liver [93% in rat livers (*16*)] makes it an excellent tracer for hepatic blood flow with PET imaging.

The purpose of this investigation was to determine whether hepatic arterial blood flow can be estimated by dynamic PET imaging employing ^{13}N-ammonia and a two-compartment kinetic model. Blood flow measurements with ^{13}N-ammonia and dynamic PET were then compared to hepatic microsphere blood flow values. The technique was then applied to normal human volunteers to determine if estimates of rHABF obtained through PET are in a range consistent with literature values and also to assess its clinical practicality.

MATERIALS AND METHODS

Animal Studies

Mongrel dogs weighing 20–30 kg were anesthetized with intravenous sodium pentobarbital (25 mg/kg), intubated, and ventilated with room air using a Harvard pump. Polyethelene catheters were advanced through femoral arteries into the abdominal aorta for withdrawal of arterial blood and monitoring of systemic blood pressure. A tygon catheter was placed in the atrial appendage for injection of radiolabeled microspheres. The anesthetized dogs were placed in a Siemens ECAT 931/08 PET scanner in the lateral position to include left ventricular cavity and the superior portion of the liver. With the last two dogs, the studies were performed with a CTI/Siemens 713 ECAT animal tomograph, with the liver in the center of the field of view. As part of a cardiac experiment, left thoracotomy was performed to allow monitoring of flow changes in the left anterior descending artery following

Received Mar. 7, 1991; revision accepted Jun. 26, 1991.
For reprints contact: Benjamin C. Chen, MD, Creighton Center for Metabolic Imaging, 901 Dorcas St., Omaha, NE 68108.

TABLE 1
Summary of Dog Intervention

Dog no.	Run no.	Intervention protocol	rHABF (ml/ming/g) PET measured	rHABF (ml/ming/g) Microsphere flow
1	a	LAD occlusion	0.13 ± 0.0005	0.15 ± 0.02
2	a	control	0.87 ± 0.03	0.90 ± 0.06
	b	dipyridamole IV infusion	0.46 ± 0.02	0.44 ± 0.05
	c	LAD occlusion	0.33 ± 0.01	0.22 ± 0.03
3	a	control	0.26 ± 0.01	0.24 ± 0.03
	b	dipyridamole IV infusion	0.46 ± 0.02	0.41 ± 0.04
4	a	control	0.22 ± 0.01	0.23 ± 0.03
	b	LAD occlusion	0.08 ± 0.002	0.03 ± 0.01
5	a	control	0.12 ± 0.01	0.14 ± 0.02
	b	dipyridamole IV infusion	0.30 ± 0.02	0.19 ± 0.02
	c	LAD occlusion	0.16 ± 0.02	0.19 ± 0.02
6	a	dipyridamole IV infusion	0.44 ± 0.02	0.31 ± 0.04
	b	LAD occlusion	0.20 ± 0.02	0.15 ± 0.02
7	a	control	0.36 ± 0.04	0.39 ± 0.04
	b	dipyridamole IV infusion	0.58 ± 0.06	0.64 ± 0.08
8	a	control	0.11 ± 0.01	0.10 ± 0.01
	b	dipyridamole IV infusion	0.22 ± 0.02	0.22 ± 0.02

With the exception of the dog in study 2, which had an unusually high baseline rHABF demonstrated by both microsphere and the dynamic PET measurement. Two studies (3 and 5) demonstrated an increase of 77% and 150% in rHABF after the infusion of dipyridamole. Study 4 showed a reduction of 64% in rHABF after acute LAD occlusion (0.08 ml/min/g) from the baseline (0.22 ml/min/g), while in study 5, where the baseline rHABF is very low (0.12 ml/min/g), there was no significant change after LAD occlusion (0.16 ml/min/g). Studies 1 through 6 were performed with ECAT 931 and the data were used to estimate p(1) in model Equation 10. Studies 7 and 8 were performed with ECAT 713 animal tomograph and the data from these two studies were used to assess the validity of the model.

pharmacologic intervention or mechanical occlusion. Monitoring of ECG lead II, systemic blood pressure and blood gases was performed throughout each experiment.

A total of 17 studies were performed in eight dogs in conjunction with cardiac blood flow experiments. The interventions listed in Table 1 were performed in addition to a baseline study at control flow. Global hyperemia was induced by constant infusion of dipyridamole (0.56 mg/kg) over 4 min in six experiments. In five experiments, regional myocardial hypoperfusion was induced using a hydraulic coronary occluder placed distally to the flow probe resulting in a reduction in cardiac output.

Nitrogen-13-ammonia (5 mCi = 185 MBq) was injected intravenously as a 30-sec slow bolus, and dynamic PET acquisition began concomitantly. Simultaneous with ^{13}N-ammonia injection, 1.5×10^6 polystyrene microspheres (15.5 ± 0.1 μm) labeled with 15 μCi of ^{46}Sc, ^{57}Co, ^{113}Sn, ^{95}Nb or ^{103}Ru were injected into the left atrium. Arterial blood samples were drawn every 10 sec for the first 2 min, and whole blood samples were immediately counted for their ^{13}N radioactivity in a scintillation well counter. The fraction of plasma activity remaining as ^{13}N-ammonia was determined biochemically at 40, 80, 120 and 180 sec after initiation of ^{13}N-ammonia infusion. Nitrogen-13-ammonia was separated from metabolites by cation exchange chromatography (Dowex AG 50W - X8, 50-100 mesh) and the fraction was counted for radioactivity in a well counter.

After the animals were killed, the livers were harvested and 12 segments of approximately 800 mg were dissected from various parts of the liver for microsphere analysis of rHABF according to:

$$\text{rHABF (ml/min/g)} = F_p \times (C_t/C_b), \qquad \text{Eq. 1}$$

where F_p is the withdrawal rate for arterial blood samples (ml/min), C_t is microsphere tissue concentration (cpm/g), and C_b is total microsphere activity in the reference arterial blood sample (*10*).

Normal Subjects

Eight healthy male human volunteers participated in this investigation. The mean age was 20 ± 2 yr (range 17–24 yr). All subjects were studied under fasting condition (≥12 hr). After giving informed consent, each subject was studied in a supine position, in a ECAT 931 whole-body scanner to allow simultaneous 15 planes image acquisition of the left ventricular cavity and superior aspect of liver. Twenty millicuries (740 MBq) of ^{13}N-ammonia in saline were injected intravenously over a 30-sec period. No blood samples were taken.

Data Acquisition

Transmission images using a ^{68}Ge filled circular ring source were obtained for correction of photon attenuation. A calibration factor was determined by comparing activity concentration, as measured by PET in a cylinder containing a uniform concentration of ^{68}Ge, with the concentration obtained by counting an aliquot of the cylinder solution in a well counter.

Dynamic PET scans were performed following an intravenous injection of ^{13}N-ammonia. The acquisition protocol consisted of twelve 10-sec frames and six 20-sec frames acquired consecutively for a total imaging time of 4 min.

Data Analysis

A Shepp-Logan filter with cutoff at 30% Nyquist frequency was used for image reconstruction, resulting in an in-plane image resolution of 10.5 mm FWHM with a slice thickness of 6.75 mm in the ECAT 930 tomograph. For the ECAT 713 tomograph, the in-plane image resolution was 6.2 mm FWHM and slice thickness was 3.37 mm. In the first 13 canine experiments and in all the human studies, hepatic tissue activity was determined by region

of interest (ROI) analysis in six areas evenly distributed in the right superior lateral aspect of the liver. The arterial input function was determined from a circular ROI centered in the left ventricular cavity of a mid-left ventricular slice (*11*). In the last four canine experiments done in the ECAT 713 animal tomograph where the liver was in the center of the field of view, ROIs were drawn over six areas evenly distributed in the mid-portion of the right and left lobes of the liver. In the canine studies, a comparison with the input function as calculated from arterial blood samples was also performed. The data from the first 13 experiments were used to estimate the parameter p(1) in the extraction fraction formula (see the following section), while the data from the last 4 experiments were used to evaluate the validity of the model.

Tracer Kinetic Modeling

A two-compartment mathematical model as shown in Figure 1 was used to fit the data. The model consists of both a free space, composed of vascular and free ammonia, and a trapped space for ^{13}N bound in tissue. The tracer kinetics of the model are described mathematically by the following equations:

$$\frac{dQf(t)}{dt} = \frac{-(K1 + rHABF)\cdot Qf(t)}{V} + k2\cdot Qt(t) + rHABF\cdot Ca(t)\cdot p \quad \text{Eq. 2}$$

$$\frac{dQt(t)}{dt} = \frac{K1\cdot Qf(t)}{V} - k2\cdot Qt(t), \quad \text{Eq. 3}$$

where Qf(t) and Qt(t) are, respectively, the total activities (cpm/pixel) in the free (Qf) and trapped (Qt) space, K1 is the forward rate constant from the free-to-trapped compartment (ml/min/g), k2 the reverse-rate constant from the trapped-to-free compartment (min^{-1}), V is the distribution volume of the tracer within the free space (ml/g), rHABF the hepatic arterial blood flow (ml/min/g), Ca(t) the arterial activity of ^{13}N-ammonia (cpm/pixel), p the specific gravity of blood (~1 g/ml), and t is time (min). The arterial input function Ca(t) was determined from a left ventricular blood-pool ROI. The liver tissue time-activity curve was obtained from the dynamic PET study: Let Y be the sum of Qt and Qf, i.e.,

$$Y = Qt(t) + Qf(t). \quad \text{Eq. 4}$$

The tissue extraction E is defined as the ratio of the extracted activity to the total activity delivered to the system. From the model, E can be shown to be:

$$E = \frac{K1}{K1 + rHABF}, \quad \text{Eq. 5}$$

Rearranging Equation 5 gives:

$$K1 = \frac{rHABF\cdot E}{1 - E}. \quad \text{Eq. 6}$$

In addition, the relationship between E and rHABF was experimentally determined in Equation 11 as described in the next section. This relationship for K1, E, and rHABF was used in conjunction with the observed arterial and tissue time-activity data in the equations. A nonlinear least squares fitting procedure was used to fit the hepatic tissue activity data, Y, to the above differential equations.

Several assumptions were made in our study:

- There was no significant portal venous contribution of ^{13}N-ammonia during the first 90 sec of scan time.
- Nitrogen-13-ammonia behaves like a freely diffusible tracer at the capillary-sinusoid interface.
- Only the initial 90 sec of time-activity data was used in the fitting routine. By limiting the data analysis to 90 sec, it was assumed that backdiffusion from trapped-to-free space is minimal, i.e., k2 = 0. A check of this assumption was made by comparing flow estimates with k2 set to 0.01/min and 0.2/min.
- A value of 0.8 ml/g was used for the free space volume of distribution, V. The effect of an inaccurate estimation of V on the final value obtained from rHABF was investigated by varying V from 0.5 ml/g to 2.0 ml/g.

The tracer kinetic modeling software BLD (*12*) was used to perform all nonlinear fitting of the model equations to the time-activity data.

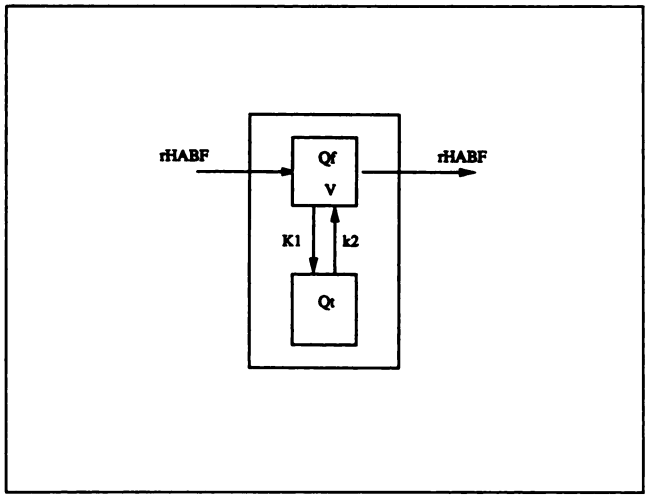

FIGURE 1. Two-compartment model for hepatic arterial blood flow, where Q(t) is the total activity (cpm/pixel) in the free (Qf) and trapped (Qt) space, K1 is the forward-rate constant from the free-to-trapped compartment (ml/min/k), k2 is the reverse-rate constant from the trapped-to-free compartment (min^{-1}), V is the distribution volume of the tracer within the free space (ml/g), rHABF is hepatic blood flow (ml/min/g), Ca(t) is the arterial activity of ^{13}N-ammonia (cpm/pixel), p is the specific gravity of blood (~ g/ml), and t is time (min). The arterial input function Ca(t) was determined from a left ventricular blood-pool ROI.

Hepatic Net Extraction of ^{13}N-Ammonia

Regional hepatic activity concentrations of tracer are a function of first-pass extraction E, rHABF and the integral of the total arterial input curve Ca(t). The hepatic activity concentration Q(T) at time T after tracer injection can be described by:

$$Q(T) = E\cdot rHABF\cdot \int_0^{T_O} Ca(t)dt, \quad \text{Eq. 7}$$

where the arterial tracer activity concentration Ca(t) is determined from the left ventricular cavity in serial cross-sectional images. Rearranging Equation 7 gives:

$$E\cdot rHABF = \frac{Q(T)}{\int_0^{T_O} Ca(t)dt}. \quad \text{Eq. 8}$$

For ^{13}N-ammonia, hepatic tissue activity was determined from the images at 90 sec, that is, the arterial input function was

integrated over the first 90 sec only. This was done because hepatic tissue activity concentration changes little thereafter. Assuming that E is a function of rHABF in the following manner as given by the Renkin-Crone equation (*13–15*):

$$E = [1 - e^{-p(1)/rHABF}], \quad \text{Eq. 9}$$

where p(1) is the permeability surface product with a unit in ml/min. By multiplying both sides of Equation 9 by rHABF, the following relationship was obtained:

$$E \cdot rHABF = rHABF \cdot [1 - e^{-p(1)/rHABF}]. \quad \text{Eq. 10}$$

Using the values of E·rHABF from the first 13 experiments calculated from Equation 8 and the values of rHABF obtained from the microsphere studies, we estimated p(1) to be 1.18 ml/min/g by nonlinear regression, as shown in Figure 2, with r^2 = 0.90. Thus, in the model, E is constrained to be related to rHABF according to the equation below:

$$E = (1 - e^{-1.18/rHABF}). \quad \text{Eq. 11}$$

Vascular Component in the Estimation of rHABF

Since the liver parenchyma is immersed in the vascular space, it is important to evaluate the effect of vascular space on the estimation of rHABF. Nonlinear regression was performed with an additional vascular component added to Equation 2 in the following way:

$$Y = Qf(t) + Qt(t) + VS \cdot Ca(t), \quad \text{Eq. 12}$$

where VS is an additional parameter (non-dimensional) denoting the vascular fraction from the arterial input function, Ca(t). VS may also represent the spillover fraction from the surrounding tissues, but since the ROI is drawn away from the heart and there are no other organs with high ^{13}N radioactivity near the liver, VS should mostly represent the vascular component within the liver parenchyma. Nonlinear regression to estimate rHABF and VS was performed using tissue and arterial time-activity curves along with Equations 2, 3, 6, 11.

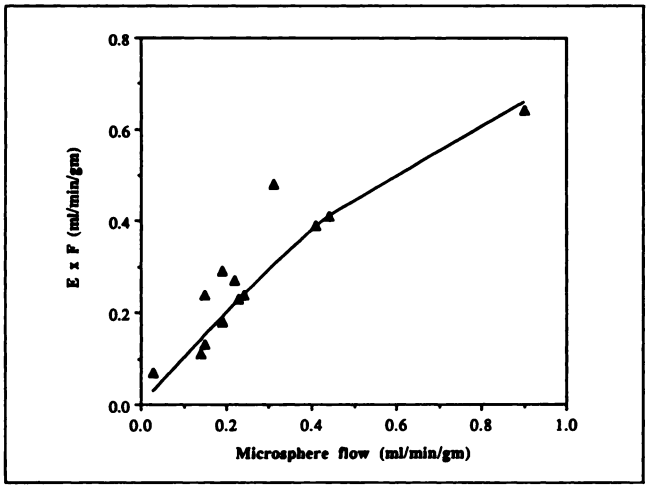

FIGURE 2. The plot of the product of extraction fraction (E) and rHABF, as obtained from dynamic PET canine studies against microsphere hepatic blood flow, to estimate p(1). The product of E·rHABF on the y-axis was obtained from Equation 8, where Q(T) is liver tissue radioactivity calculated from dynamic PET imaging, and Ca(t) the input function obtained from left ventricular cavity time-activity curves. rHABF on the x-axis was obtained from the microsphere studies. Nonlinear regression of the plot yields a p(1) estimate of 1.18 ml/min/g, s.e. = 0.24 ml/min/g, and r^2 = 0.83.

RESULTS

Kinetic Behavior of Ammonia in Liver

Figure 3A-B shows ^{13}N-ammonia PET images for a normal volunteer and a dog, respectively. Uptake and retention of the tracer in the liver parenchyma gradually increased. Representative regional time-activity curves generated by using ROIs over the canine liver tissue and the left ventricular cavity are shown in Figure 4. The concentration of ^{13}N increases for approximately 90 sec. The hepatic level of ^{13}N-ammonia plateaus after the initial rise and remains relatively constant thereafter.

Estimates of Liver Blood Flow

Hepatic arterial blood flows from the canine experiments were estimated by fitting the time-activity curves with the model for each study (see Methods). A typical curve fitted to the liver time-activity curve is shown in Figure 5, with high correlation coefficient (0.95) and fast convergence (less than five iterations for convergence criteria set at 0.1%). A summary of calculated rHABF versus microspheres (MS) data in the first 13 experiments are shown in Figure 6. Linear regression yields rHABF = 0.95 × MS + 0.04 (r = 0.97, residual sum of squares, RSS_{13},

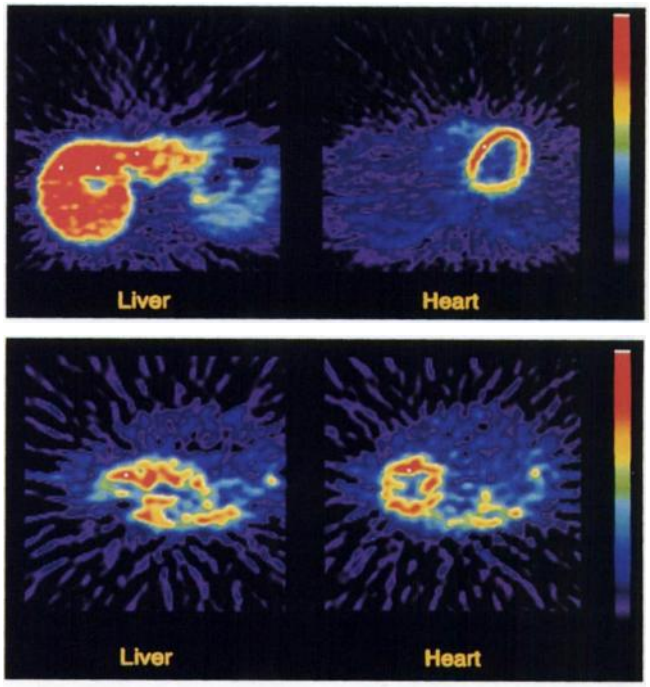

FIGURE 3. (A) PET images of the liver (left) and left ventricular cavity (right) in a normal volunteer at 220–240 sec/frame. The rHABF estimate in this subject is 0.30 ml/min/g. The crescent shape activity in the right lower corner of the liver image is the spleen. (B) PET images of the liver (left) and left ventricular cavity (right) in a dog at 220–240 sec. The rHABF and myocardial blood flow estimates in this study are 0.87 ml/min/g and 1.34 ml/min/g, respectively.

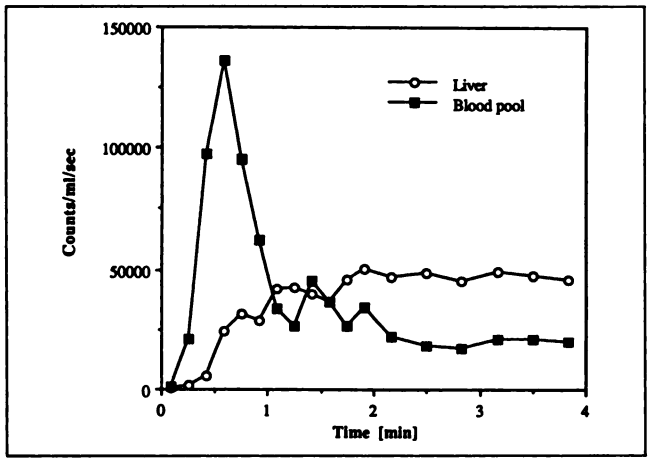

FIGURE 4. Time-activity curve for canine blood-pool and hepatic tissue. Note that the liver curve rises and plateaus at 1.5 min, at which time the blood-pool time-activity curve has already cleared.

equals 0.037). To test the validity of the approach, we applied the model to dynamic PET data from the last four experiments. Comparison with the simultaneous microsphere rHABF is also shown in Figure 6, with linear regression showing rHABF = 0.87 × MS + 0.02 (r = 0.98, RSS_4 = 0.001). To examine if there was significant difference between the two lines, the residual sum of squares of the linear regression of the combined line (RSS_{17}) was obtained, and the F-ratio

$$\frac{\{RSS_{17} - (RSS_{13} + RSS_4)\}/2}{(RSS_{13} + RSS_4)/\text{d.f.}},$$

(where d.f. represents the degree of freedom, 13) was calculated to be 1.23. At 95% confidence level (α = 0.05), the above F-ratio showed no significant difference among the combined line and each separate line. When the two sets of data were combined into one, linear regression yields rHABF = 0.04 + 0.92 × MS, r = 0.98.

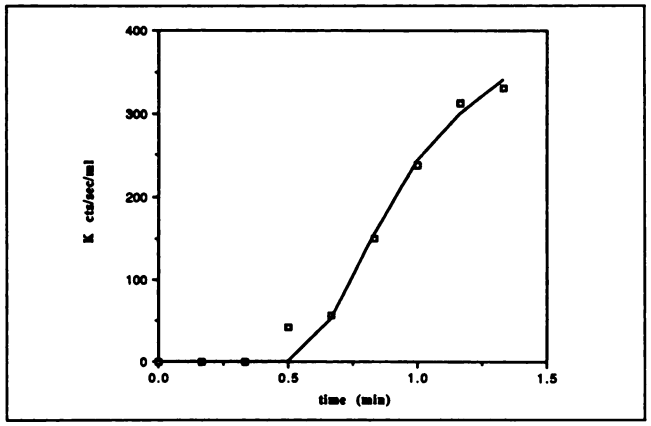

FIGURE 5. A human hepatic tissue time-activity curve (squares) from the same subject as in Figure 3A, and the fitted curve (solid line) obtained from the two-compartment model, with r^2 = 0.98, and s.e. = 0.01.

Extraction fraction estimates, E, were greater than 90% in all human and canine studies except for the one canine experiment with exceptionally high rHABF (0.87 ml/min/g), which yields extraction fraction of 79%. To test the sensitivity of the estimates on the parameter p(1), canine rHABF estimates were recalculated with ±10% change in the value of p(1) used in Equation 10, which resulted in 1.2% ± 5.2% decrease or 3.7% ± 4.4% increase in rHABF estimates, respectively. Since microsphere flow value is not obtainable in humans, we used 1.18 as the estimate for p(1) derived from canine studies to calculate rHABF in eight normal human volunteers, yielding a value of 0.26 ± 0.07 ml/min/g.

Effects of Correction for Metabolites on Flow Determination

Nitrogen-13-ammonia is rapidly metabolized to urea and glutamine in several organ systems (*16,17*) and arterial blood activity represents a mixture of ^{13}N-labeled ammonia, urea and glutamine. Comparison of the input functions for the dog studies with and without metabolite correction is shown in Figure 7. Our canine studies showed an average of 69% of total radioactivity as ammonia at 2 min after injection, which is comparable to literature values [81% ± 17%, (*17*)]. To evaluate the effect of correcting for ^{13}N-metabolites in blood on hepatic blood flows and rate constant estimates, results obtained from curve fitting with and without a correction factor for ^{13}N-ammonia were compared. rHABF estimates were underestimated by including ^{13}N-metabolites in blood by 4.1% ± 0.66% in canine studies.

Effects of the Volume of Distribution on Flow Determination

Varying the volume of distribution for $^{13}NH_3$ within the range of 0.5 to 2.0 ml/g resulted in less than 6% variation in the estimated value of rHABF. Over the range of the

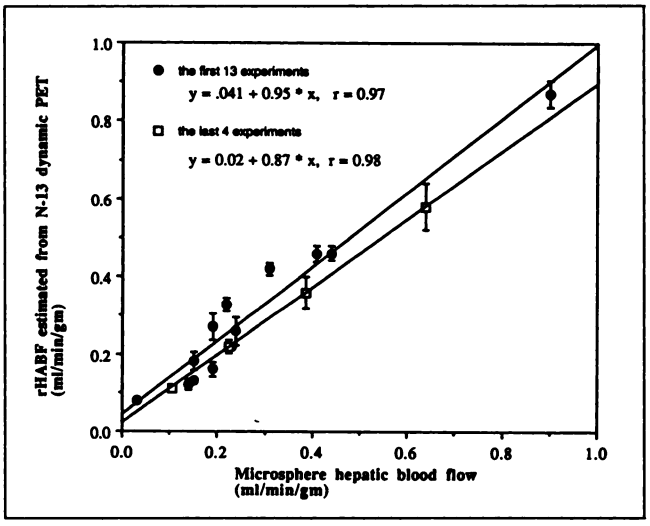

FIGURE 6. rHABF estimated from PET versus values obtained from microspheres in the first 13 and the last 4 canine studies. The standard errors are larger at higher flow.

expected k2 values (0 to 0.2 min^{-1}), there is less than a 2% increase in rHABF estimates. The effect on the rHABF estimate, when varying either V or k2, is similar at both high and low perfusion values.

Effect of Vascular Space on Flow Determination

Adding a vascular component as in Equation 12 in the estimation of rHABF results in an average of 5.5% ± 9.0% variation in the flow estimates. The average of the vascular component factor estimate, VS, is 0.025.

Comparison of Estimation of Flow Using Left Ventricular Cavity (LVC) Time-Activity Curve Versus Arterial Blood Samples

Comparison of flow estimates using LVC versus arterial blood samples in the canine studies demonstrates an average difference of 4.3% ± 7.8%.

DISCUSSION

Method Validation

The liver is a fairly homogeneous organ at the macroscopic level, even though it has long been established that there are different populations of hepatocytes, including periportal hepatocytes (near the sinusoidal inflow) and perivenous hepatocytes (near the sinusoidal outflow) (*18*). Each carries different sets of enzymes and behaves in a metabolically different manner. For our purposes, since these populations are very well intermixed within the liver parenchyma, they would not be differentiable with the spatial resolution of the current tomograph. Thus, it appears appropriate to consider the liver a homogeneous organ. In addition, blood flow within the liver appears to be uniformly distributed, as previously indicated by the even distribution of microspheres injected into either the hepatic artery or the portal vein (*19*). Since only the first 90 sec of the study was used for the estimation of rHABF,

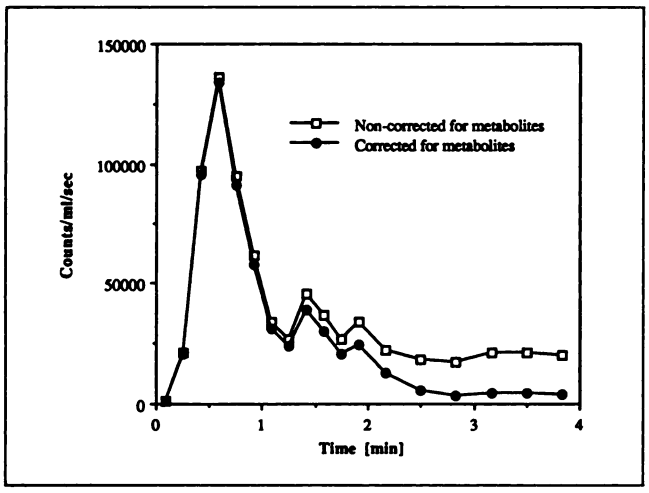

FIGURE 7. Comparison of left ventricular input function with and without metabolite correction in a canine study. Note that in the first 2 min of study there are relatively small differences between the two curves, and the rHABF estimates show a 3% difference.

no significant activity is expected to be in the biliary tree. Moreover, when the vascular space is taken into account, estimates of rHABF vary only 5.5%, with a small vascular component (an average of 2.5%). Thus, it is reasonable to use the average rHABF estimated from ^{13}N-ammonia for comparison with the average flow value obtained from the microsphere study in order to demonstrate the feasibility of estimating regional hepatic blood flow in both canine and human liver with ^{13}N-ammonia and dynamic PET imaging. By using a simple two-compartment tracer kinetic model, isolation of the initial tracer extraction by the liver tissue from subsequent metabolic radionuclide trapping in the form of ^{13}N-glutamine can be achieved. In the last 4 experiments, the surface permeability product, p(1), obtained from the first 13 experiments was used to estimate rHABF, which showed good correlation with microsphere flow values (rHABF = 0.02 + 0.87 × MS, r = 0.98). This was not significantly different from the value obtained from the first 13 experiments, which further supports the validity of the model.

In this study, we assumed that there was no significant contribution to tissue radioactivity from portal venous flow in the first 90 sec, even though portal vein constitutes about two-thirds of total liver blood flow. This is based on the following reasoning. First, if there was significant portal contribution of ^{13}N-ammonia to the liver during the first 90 sec, the product of flow and extraction fraction should be greater than rHABF calculated from microspheres, due to the high extraction fraction of ^{13}N-ammonia in the liver and the relative slow clearance of the label from the liver as shown by Freed et al. (*20*) and by our measurements. However, the present results showed the opposite, with E·F values slightly less than microsphere rHABF (Fig. 2), which supports our hypothesis that the contribution of portal supply is insignificant during the first 90 sec of the study. Second, the high intestinal extraction [close to 100%, (*20*)] suggests there may be significant delay and dispersion of ammonia through the intestinal mucosa; the radioactivity level in the portal venous flow is not expected to be significant during the first 90 sec. Third, ammonia is highly extracted by the spleen (~80%) (*20*) and therefore little ^{13}N radioactivity return from the splenic vein is expected in the first 90 sec. Fourth, unlike the findings of Freed et al. (*20*), our estimate of rHABF correlates very well with the microsphere value, which only measures HABF. In addition, our estimates of rHABF in human (0.26 ± 0.07 ml/min/g) were comparable with direct measurement of HABF with intra-operative electromagnetic flow probes in surgical patients (*21*) that reported an average value of 308 ml/min in eight patients without liver disease. Assuming an average liver mass of 1350 g (*22*), the above value yields rHABF of 0.23 ml/min/g.

The estimate of rHABF using the two-compartment model in our study proved relatively insensitive to errors in the assumed value of the volume of distribution (V) for $^{13}NH_3$ in the free space, as well as to errors in the assumed

value of k2. In only one experiment, where rHABF was unusually high (0.87 ml/min/g by PET, and 0.9 ml/min/g by the microsphere study), did varying V from 0.5 ml/g to 2.0 ml/g cause a significant variation in rHABF (13%). In the low to moderately high range of rHABF (from 0.08 cc/min/g to 0.44 ml/min/g), varying V in uniform steps of 0.3 ml/g from 0.5 ml/g to 2.0 ml/g resulted in less than a 6% variation in the estimates. This suggests that the estimation algorithm is stable within the physiologic range of V over the duration of the study. Similarly, varying k2 from 0 to 0.1 and 0.2 min^{-1} caused less than a 2% variation in the estimate of rHABF. This was expected, since the backdiffusion of NH_3 in the liver does not appear to be significant in the first 90 sec of the study. In addition, our studies confirm the validity of using a left ventricular cavity time-activity curve as the input function, showing insignificant changes in flow estimate using arterial blood samples.

Since it is not possible to obtain tissue microsphere data for human studies, the p(1) value estimated from canine studies was used to calculate rHABF in humans. The estimates appeared insensitive to p(1), since a 10% change in p(1) resulted in only 3.7 ± 4.4% variation in rHABF. Moreover, the estimates of rHABF in normal human volunteers agreed with the literature value as discussed above, further confirming the practical utility of the p(1) value used.

Dipyridamole is a vasodilator that acts predominantly on small resistance vessels in the coronary bed. It has been shown that dipyridamole acts on the hepatic arterial beds by amplifying the dilation induced by exogenous adenosine effects and by increasing the magnitude of the hepatic arterial buffer response (*23*). It has also been demonstrated that adenosine produces dilatation of the hepatic artery (*24*), and the "adenosine washout hypothesis" has been proposed as a mechanism for intrinsic hepatic arterial blood flow regulation (*1*). In our study, with the exception of dog number 2, which had an unusually high baseline rHABF demonstrated by both the microsphere measurement and the dynamic PET measurement, two other experiments demonstrated an increase of 77% and 150% in rHABF after dipyridamole infusion, which is consistent with the reported effects of dipyridamole on hepatic arterial flow.

It has been observed that in acute circulatory failure there may be a transient increase in transaminase (ischemic hepatitis). If prolonged, there may be permanent zone 3 necrosis (cardiac cirrhosis). In our study, one experiment showed a reduction of 64% in rHABF after acute LAD occlusion (0.08 ml/min/g) from the baseline (0.22 ml/min/g), while in another study where the baseline rHABF is very low (0.12 ml/min/g), there was no significant change after LAD occlusion (0.16 ml/min/g). These data are consistent with the hypothesis that an impairment in visceral arterial flow may contribute to hepatic dysfunction in circulatory failure.

Nitrogen-13-Ammonia as a Flow Tracer for rHABF

Detailed comparisons of various tracers for myocardial blood flow, i.e. ^{13}N-ammonia, ^{15}O-water and ^{82}Rb, have been reported (*4–7*). The "ideal" blood flow tracer should be highly extracted by the tissue of interest. Such tissue retention should be approximately proportional to flow over a wide range of values. It has been shown that 93% of ^{13}N-ammonia is extracted in the first pass in rat liver (*16*), while the bulk of the tracer is removed from the blood within 1–2 min from injection in the rat study. The metabolism of ammonia in the liver is extremely rapid ($t_{½}$ ~ 5 sec), with ^{13}N-ammonia being converted into glutamine, aspartate and urea. However, the trapping is reversible due to the glutamine dehydrogenase reaction, and it is not possible to decide whether the reaction results in a net synthesis or a net removal of ammonia from the liver.

In our studies, ^{13}N activity shows a steady rise to peak concentration in both human and canine livers between 1 and 2 min from the bolus injection of ^{13}N-ammonia. In addition, the two-compartment rHABF model yields high extraction fraction estimates for both the canine and human studies, with rHABF estimates in canine studies correlating well with microsphere results. This evidence supports the conclusion that ^{13}N-ammonia is a suitable hepatic blood flow tracer.

Metabolic Correction of ^{13}N Blood Activity

Nitrogen-13 ammonia is rapidly metabolized in several organs, resulting in the appearance of labeled metabolites in plasma (*16*). Therefore, a correction factor for the contamination of the arterial input function was applied. Data from this study demonstrate that blood flow values show only a slight dependence on ^{13}N metabolite correction, since rHABF estimates are obtained from the tracer kinetics during the initial 90 sec after the injection of ^{13}N-ammonia. At this time, little metabolic contamination of the arterial input function is expected [(*18,25*) and Fig. 7]. This indicates the clinical practicality of the present approach without the need for ^{13}N-ammonia metabolite correction.

Technical Considerations

The liver appears to be an organ very suitable for PET imaging due to its large size, homogeneity, and relative absence of motion. Image reconstruction can be performed with a filter of low cutoff frequency, corresponding to low noise level in the final image. Further improvement in statistics may be obtained by summing together several image planes. In current PET scanners, the axial field of view (FOV) allows only a 10-cm long section of the patient or animal to be simultaneously imaged. If one wishes to image the liver over its entire length, it is likely that the left ventricular cavity would fall outside the FOV. For this reason, we are currently investigating the use of the abdominal aorta for arterial input function determination.

CONCLUSIONS

Dynamic PET imaging with ^{13}N-ammonia allowed the quantitative assessment of rHABF, which correlated well with values obtained by independent microsphere technique (rHABF = 0.92 × MS + .04, r = 0.98) in canine studies under various flow conditions. The same quantification performed on normal human volunteers yields a mean rHABF of 0.26 ± 0.07 cc/min/g, which is in agreement with the literature values. Further studies in patients with severe hepatocellular disease but normal cardiac output as compared to patients with normal liver function but low cardiac output will be needed to show the interrelationship of the pump and blood flow reserve.

ACKNOWLEDGMENTS

This work was supported in part by the Department of Energy, Office of Health and Environmental Research, Washington, DC, and grant DE-FCO3-87-ER6015 from the National Institutes of Health, Bethesda, Maryland. The authors would like to thank Ronald Sumita, Lawrence Pang, and Herb Hanson for their technical assistance.

REFERENCES

1. Lautt WW, CV Greeway. Conceptual review of the hepatic vascular bed. *Hepatology* 1987;7:952–963.
2. Johnson DJ, Muhlbacher F, Wilmore DW. Current research review: measurement of hepatic blood flow. *J Surg Res* 1985;39:470–481.
3. Fleming JS, Avkery DM, Walmsley BH, et al. Scintigraphic estimation of arterial and portal venous components of liver perfusion. *J Nucl Med* 1983;22:18–21.
4. Hoffman EJ, Huang SC, Phelps ME. Quantitation in positron emission computed tomography. I. Effect of object size. *J Comput Assist Tomogr* 1979;3:299–308.
5. Schelbert HR, Phelps ME, Huang SC, et al. N-13-ammonia as an indicator of myocardial blood flow. *Circulation* 1981;63:1259–1272.
6. Hutchins GD, Schwaiger M, Rosenspire KC, et al. Noninvasive quantification of regional blood flow in human heart using N-13 ammonia and dynamic positron emission tomography imaging. *J Am Coll Cardiol* 1990;15:1032–1042.
7. Bergman SR, Fox K, Ranf AL, et al. Quantification of regional myocardial blood flow in vivo with $H_2{}^{15}O$. *Circulation* 1984;70:724–733.
8. Shea MJ, Wilson RA, deLandsheere CM, et al. Use of short- and long-lived rubidium tracers for the study of transient ischemia. *J Nucl Med* 1987;28:989–997.
9. Smith JJ. Role of positron emission tomographic scanning in the diagnosis of liver disease. *Semin Liver Dis* 1989;9:86–89.
10. Heymann MA, Payne BD, Hoffman JIE, et al. Blood flow measurement with radionuclide-labeled particles. *Prog Cardiovasc Dis* 1977;20:50–60.
11. Weinberg IN, Huang SC, Hoffman EJ, et al. Validation of PET-acquired input functions of cardiac studies. *J Nucl Med* 1988;29:241–247.
12. Carson RE, Huang SC, Phelps ME. BLD, a software system for physiological data handling and data analysis. *Proceedings of the Fifth Annual Symposium on Computer Applications in Medical Care.* New York: IEEE;1981:562–565.
13. Kety SS. The theory and applications of inert gas at the lung and tissues. *Pharmacol Rev* 1951;3:1–41.
14. Renkin EM. Transport of potassium-42 from blood to tissue in isolated mammalian skeletal muscles. *Am J Physiol* 1959;197:1205–1210.
15. Crone C. Permeability of capillaries in various organs as measured by use of the 'indicator diffusion' method. *Acta Physiol Scand* 1963;58:292–305.
16. Cooper AJL, Nieves E, Coleman AE, Filc-DeRicco S, Gelbard AS. Short-term metabolic rate of [N-13]ammonia in rat liver in vivo. *J Biol Chem* 1987;262:1073–1080.
17. Rosenspire KC, Schwaiger M, Mangner TJ, et al. Metabolic fate of N-13-ammonia in human and canine blood. *J Nucl Med* 1990;31:163–167.
18. Haussinger D. Nitrogen metabolism in liver: structural and functional organization and physiological relevance. *Biochem J* 1990;267:281–290.
19. Greenway CV, G Oshiro. Intrahepatic distribution of portal and hepatic arterial blood flows in anesthetized cats and dogs and the effects of portal occlusion, raised venous pressure and histamine. *J Physiol* 1972;227:473–485.
20. Freed BR, Gelbard AS. Distribution of N-13 following intravenous injection of [N-13]ammonia in the rat. *Can J Physiol Pharmacol* 1980;60:60–67.
21. Schenk WG, McDonald JC, McDonald K, et al. Direct measurement of hepatic blood flow in surgical patients: with related observations on hepatic flow dynamics in experimental animals. *Ann Surg* 1962;156:463–471.
22. Sherlock S. *Diseases of the liver and biliary system.* New York: Blackwell; 1989:1.
23. Lautt WW, Legare DJ, d'Almeida MS. Adenosine as putative regulator of hepatic arterial flow (the buffer response). *Am J Physiol* 1985;248:H331–H338.
24. Lautt WW, Legare DJ. The use of 8-phenyltheophylline as a competitive antagonist of adenosine and an inhibitor of the intrinsic regulatory mechanism of the hepatic artery. *Can J Physiol Pharmacol* 1985;63:717–722.
25. Gambir SS, Schwaiger M, Huang SC, et al. A simple noninvasive quantification method for measuring myocardial glucose utilization in humans employing positron emission tomography and F-18-deoxyglucose. *J Nucl Med* 1989;30:359–366.

EDITORIAL

The Development and Application of Mathematical Models in Nuclear Medicine

The introduction and application of more sensitive and specific radiopharmaceuticals is a major component of scientific progress in nuclear medicine. Each tracer is targeted to measure a certain physiologic parameter of interest (e.g., blood flow, metabolism, receptor content) in one or more organs or regions. PET and SPECT instrumentation can produce high quality three-dimensional images of the radioactivity distribution of each tracer. With proper corrections for the various physical effects in emission tomography (e.g., attenuation, scatter), quantitatively accurate measurements of regional radioactivity concentration can be obtained. These quantitative images of tracer distribution can be useful, both clinically and scientifically. The use of tracer kinetic modeling techniques, however, can substantially improve their quality and utility (*1*). The model defines the quantitative connection between the radioactivity levels and all of the physiologic parameters that affect the uptake and metab-

Received Aug. 15, 1991; accepted Aug. 15, 1991.

For reprints contact: Richard E. Carson, PhD, PET Department, NIH, Building 10, Room 1C-401, Bethesda, MD 20892.